Materials Chemistry and Physics 262 (2021) 124284

Contents lists available at ScienceDirect

Materials Chemistry and Physics

journal homepage: www.elsevier.com/locate/matchemphys

Structural, electronic and optical modeling of perovskite solar materials $ASnX_3$ (A = Rb, K; X = Cl, Br): First principle investigations

Karina Khan [a], Jagrati Sahariya [b,**], Amit Soni [c,*]

[a] Department of Physics, Manipal University Jaipur, Jaipur, 303007, Rajasthan, India
[b] Department of Physics, National Institute of Technology, Srinagar (Garhwal), 246174, Uttarakhand, India
[c] Department of Electrical Engineering, Manipal University Jaipur, Jaipur, 303007, Rajasthan, India

HIGHLIGHTS

- Investigation of optoelectronic properties of $ASnX_3$ (A = Rb, K); (X = Cl, Br).
- Dielectric tensors are explained using transitions in energy bands.
- Explored the possible utilization in Photovoltaic and optoelectronic devices.
- Compared obtained absorption spectra with that of $MAPbI_3$.

ARTICLE INFO

Keywords:
Density functional theory
Semiconductor compounds
Optical properties
Solar cells

PACS No:
71.15. Mb
71.20. Nr
78.20.−e
88.40.H−

ABSTRACT

In this paper, we present structural, electronic and optical response for inorganic lead-free tin halide perovskites $ASnX_3$ (A = Rb, K; X = Cl, Br) compounds, to examine their possible utilization as future photovoltaic materials. The structural optimization, energy band structure, density of states and exhaustive optical spectra for these perovskite compounds are delved using the Tran-Blaha modified Becke-Johnson exchange and correlation potential as implemented in Wien2k code. Optical performance of the compounds is accomplished through the investigation of real & imaginary dielectric tensor components, optical absorption, reflectivity and refractivity spectra. Direct band gap for $RbSnCl_3$ ($RbSnBr_3$) and $KSnCl_3$ ($KSnBr_3$) compounds is obtained as 1.46 (0.98) eV and 1.48 (0.93) eV, respectively which lies within standard photo-voltaic range. Results obtained in present computations are in decent agreement with earlier reported data, which firmly endorse the accuracy of present calculations. In addition, band gap reduction is perceived while switching from X = 'Cl' to 'Br' which has also revealed the enhancement in integrated absorption coefficient. Promising electronic and optical properties obtained for these perovskite compounds affirms their potential utilization in photo-voltaic and other opto-electronic applications.

1. Introduction

Global increase in energy consumption and other severe environmental issues associated with conventional sources, has blown an alarm for research community to explore long term sustainable alternatives. Renewable sources are considered as prominent hassle-free preferred solution and amongst all available non-conventional sources, solar energy is universally chosen as most dominant source for desired energy production. Solar cells, as employed in harvesting solar energy, plays major role towards accomplishment of efficient energy production. Developing novel solar materials having features such as, lower cost, efficient generation capacity, eco-friendly nature and universal compatibility are prime objectives elaborated amongst all previous calculations [1,2]. In this context, emerging perovskite photovoltaic materials have recently gained tremendous interest due to their economic, efficient and multifunctional optical features [3–5]. The halide perovskites, especially, lead based perovskites, revealed good power conversion efficiencies and hence can be utilized for various opto-electronic applications such as, photovoltaics, light emitting diodes, sensors, lasers and radiation detectors. Therefore, these perovskites have been studied extensively to realize their structural,

* Corresponding author.
** Corresponding author.
E-mail addresses: jagrati.sahariya@gmail.com (J. Sahariya), amitsoni_17@yahoo.co.in (A. Soni).

https://doi.org/10.1016/j.matchemphys.2021.124284
Received 3 June 2020; Received in revised form 26 November 2020; Accepted 13 January 2021
Available online 16 January 2021
0254-0584/© 2021 Elsevier B.V. All rights reserved.

electronic, optical, transport properties and charge carrier mobilities. Amongst all the halide perovskites, Phenyl-ethyl-ammonium (PEA), lead-halide perovskites $(PEA)_2PbI_4$, $CH_3NH_3SnX_3$ (X = Cl, Br and I), $CsAX_3$ (A = Pb, Sn; X = Cl, Br), Cs_2PbI_4, $CsPbI_4$, $CsPbBr_3$ $Cs_2Ag_xCu_{1-x}In_yTb_{1-y}Cl_6$ and $Cs_2AgInCl_6$ have been widely investigated using various experimental and theoretical approaches. These compounds are reported to be suitable for photoluminescence, photovoltaic, infrared detection applications [6–12] and hence, have shown new dimensions to researchers. The major drawback with these lead-based perovskites is the toxic nature of the lead, which is certainly extremely hazardous for mental development, human growth and for the whole environment [13]. Effective alternate solution to this problem may be attained by substituting toxic element Pb with similar group environment friendly material 'Sn' [14,15]. Further, amazing opto-electronic properties of perovskite materials with general formula 'ABX_3', (where, 'A' = Monovalent cation, 'B' = Divalent metal cation and 'X' = Anion), has currently shown the new horizon for future photo-voltaic applications [16,17]. Density functional theory (DFT) computations for lead free halide perovskite $AGeI_3$ (A = Cs, MA, PA) compounds have been reported by Krishnamoorthy et al. [18], to demonstrate their potential candidature for photo-voltaic applications. Korbel et al. [19] have investigated the photo-voltaic, piezo-electric and magnetic behavior of ABX_3 compounds. Their investigations have shown the extraordinary competency of these compounds in related practical applications. Phase transition for a series of ABX_3 oxide, bromide, and iodide-based perovskite materials have been examined by Young and Rondinelli [20], to understand better arrangements and preferable rotation patterns. Travis et al. [21] have critically accessed tolerance or stability factor for inorganic and hybrid perovskite compounds, to explore their potential as future solar cell absorbers. Using first principle computations, Gou et al. [22] have investigated the optical performance of inorganic perovskite $CsSnI_3$ compounds. Jung et al. [23] have studied the opto-electronic properties of lead-free inorganic perovskite $(Rb,Cs)SnI_3$ materials for the desired high efficiency solar cell applications. First principle investigations for inorganic lead-free metal halide perovskite materials, $(K, Rb)SnCl_3$, have been performed by Mao et al. [24] and their results affirms the fruitful utilization of these compounds for photo-voltaic applications. Jiang et al. [25] have reported $Rb_yCs_{1-y}Sn(Br_xI_{1-x})_3$ perovskite compounds as potential candidates for solar photo-voltaic applications. Jain et al. [26] have explicitly used DFT approach for $RbSn(Cl,Br)_3$ perovskite materials and obtained promising band gap for these materials which directs their reasonable utilization for photovoltaics (PV). Yunsheng et al. [27] have examined structural, electrical and optical properties of $RbSnCl_3$ using DFT investigations and have elaborated role of strain in band gap tuning. Mechanical, optical and thermodynamic properties for Cesium based bromides are elucidated by Mahmood et al. [28] adopting DFT computations. Benyahia et al. [29] have illustrated high stability and ideal suitability of $RbSnBr_3$ perovskite compounds especially for potential solar cell applications. Rapid growth of organic-inorganic hybrid halide lead perovskite solar cells has been precisely reviewed by Yi et al. [30] due to their higher absorption and adjustable band gap properties. Yang et al. [31] have reported the systematic assessment of lattice dynamics instabilities for several inorganic perovskites having ABX_3 composition and discovered octahedral leaning as the most dominant instability for these. Very recently, Kar and Körzdörfer have performed the DFT based calculation on a series of ABX_3 type inorganic halide perovskite to identify the suitable materials for solar cell applications [32].

In present work, we have performed the systematic computations for lead-free perovskite $ASnX_3$ (A = Rb, K; X = Cl, Br) solar materials to elucidate their structural, electronic and optical behavior and to highlight their potential in future photo-voltaic applications. All calculations are performed by using the full potential linearized augmented plane wave (FP-LAPW) method within the framework of Wien2k code. Further, investigations performed in present work includes, in-depth study for structural, electronic and optical features of chosen perovskite materials by adopting the most precise Tran-Blaha modified Becke-Johnson (TB-mBJ) exchange and correlation potential. Structural, electronic and optical properties of studied compounds are explained in terms of structural optimization, energy band structure, total & partial density of states (DOS), real & imaginary dielectric tensor, optical absorption, reflectivity, and refractivity spectra.

2. Computational details

The structural, electronic and optical properties of lead-free tin halide perovskite $ASnX_3$ (A = Rb, K; X = Cl, Br) compounds are performed using the full potential linearized augmented plane wave (FP-LAPW) method as embodied in Wien2k code [33]. It is worth mentioning that in this method, solution for well-known Kohn-Sham equation [34] for a periodic crystal system is presented as:

$$\psi_k = \sum_n c_n . \varphi_{k_n} , \tag{1}$$

here, 'ψ_k' is the wave function, 'k_n' stands for the reciprocal lattice vector and 'c_n' represents coefficient of Rayleigh-Ritz vibrational principle respectively. Further, it is worthwhile that the accuracy of the results depends upon the choice of the exchange correlation functional. The exchange correlation functional potential operator is defined as [34]:

$$V_{XC}\ (\mathrm{r}) = \frac{\delta\, E_{XC}[\rho(r)]}{\delta\, \rho(r)}, \tag{2}$$

Present computations are performed using Perdew-Burke-Ernzerhof Generalized Gradient (PBE-GGA) [35] and Tran-Blaha modified Becke-Johnson (TB-mBJ) [36] approximations. Results obtained are more precise for TB-mBJ [37] calculations and hence considered for systematic elaboration. Exchange and correlation potential for this accurate TB-mBJ approximation is represented as:

$$V_{x,\sigma}^{TB-mBJ}(r) = cV_{x,\sigma}^{BR}(r) + (3c-2)\frac{1}{\pi}\sqrt{\frac{5}{6}}\sqrt{\frac{t_\sigma(r)}{\rho_\sigma(r)}}, \tag{3}$$

here, $V_{x,\sigma}^{BR}(r)$represents Becke-Rousseal potential; '$\rho_\sigma\ (r)$' is density of electrons; 'c' and '$t_\sigma\ (r)$' are the exchange correction parameter for band gap accuracy and kinetic energy density respectively.

For the computations of electronic and optical properties of cubic $ASnX_3$ (A = Rb, K; X = Cl, Br), the basic input parameters such as, lattice constants and Wyckoff positions were primarily taken from previous reported work [26] with the space group $Pm\overline{3}\ m$. To achieve the desired accuracy for all the studied properties, firstly, energy v/s volume optimization calculations were performed for all the studied compounds. Obtained optimized lattice parameters along with the available theoretical parameters and Wyckoff positions are collated in Table 1. It may be noted that there are no available experimental data on lattice parameters for the studied compounds. However the optimized lattice

Table 1
Optimized lattice parameters and Wyckoff positions for cubic $ASnX_3$ (A = Rb, K); (X = Cl, Br).

Perovskite Compounds	Optimized Lattice Parameters (Å)	Available Lattice Parameters (Å)	Wyckoff Positions			
			Atom	x	y	z
$RbSnCl_3$	5.596		Rb	0	0	0
		5.596 [26]	Sn	0.5	0.5	0.5
			Cl	0.5	0.5	0
$RbSnBr_3$	5.891		Rb	0	0	0
		5.863 [26]	Sn	0.5	0.5	0.5
			Br	0.5	0.5	0
$KSnCl_3$	5.596		K	0	0	0
		–	Sn	0.5	0.5	0.5
			Cl	0.5	0.5	0
$KSnBr_3$	5.873		K	0	0	0
		–	Sn	0.5	0.5	0.5
			Br	0.5	0.5	0

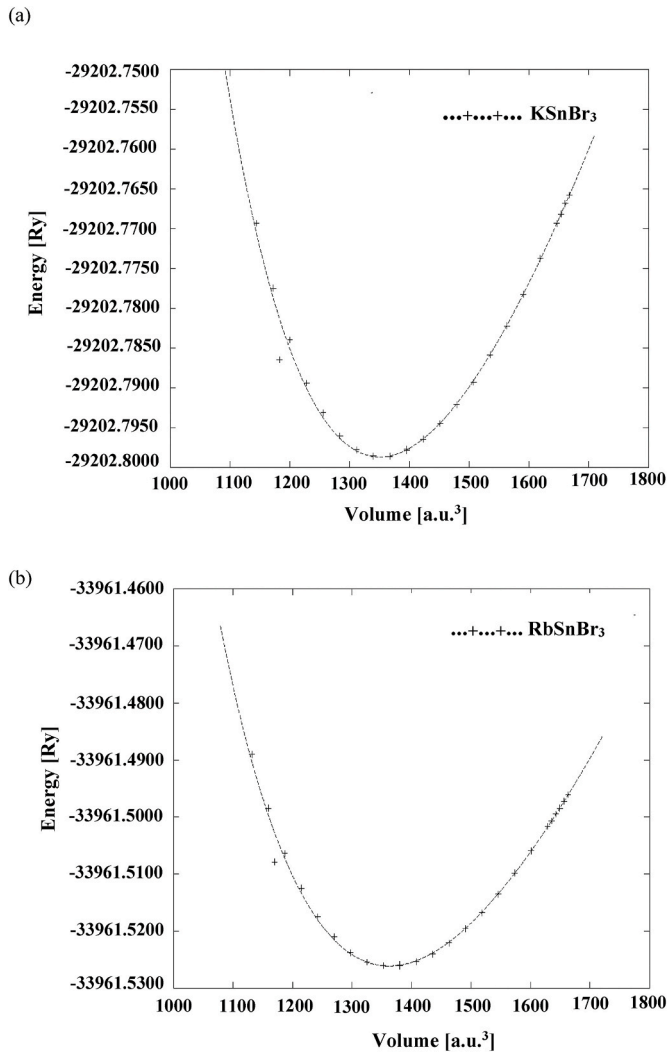

Fig. 1. Energy v/s volume optimization curves for (a) $RbSnBr_3$ and (b) $KSnBr_3$.

parameters for $RbSnX_3$ (X = Cl, Br) are in close agreement with the available theoretical parameters which affirms the accuracy of calculations. These parameters are further utilized for desired computations of different properties of studied materials. Energy v/s volume optimization curves are plotted for all compounds and results for more responsive (Rb,K)$SnBr_3$ are presented in Fig. 1 (a, b). Crystal structure and corresponding Brillouin zone (BZ) for all studied materials are represented in Fig. 2 (a, b). Minimum values for radius of muffin-tin (R_{MT}) spheres for Rb, K, Sn, Cl and Br were taken to be 2.5, 2.5, 2.5, 2.5 and 2.43 a.u. respectively. Further, plane wave functions were distend up to $R_{MT} \times K_{MAX} = 7.0$, where '$R_{MT}$' represents radius of muffin-tin (MT) radius of non-overlapping atomic sphere which is the smallest size neutral atoms and 'K_{MAX}' represents the largest value of the reciprocal lattice vector [38]. Other constraints considered in present computations include variables such as: $G_{MAX} = 12.0\ (\text{a.u.})^{-1}$, $l_{\max} = 10.0$, 1000 k points. To affirm the accuracy of calculations, cutoff values for energy, forces and core and valence state's separation were kept as 0.0001 Ry, 1 mRy/a.u and −6.0 Ry, respectively.

3. Results and discussion

3.1. Energy band structure and DOS

As discussed in previous section, we have performed the comprehensive investigations to compute structural parameters for tin based perovskite $ASnX_3$ (A = Rb, K; X = Cl, Br) materials, using the most accurate exchange and correlation functionals. Further, the calculations are performed to determine the energy band gap, electronic response and energy band structures of all the studied compounds. Electronic structure of the compounds obtained within the framework of TB-mBJ calculations are represented in Fig. 3(a–d). All the investigations are performed adopting both PBE-GGA and TB-mBJ schemes and obtained band gaps are collated in Table 2 along with previous reported results. Results obtained indicates close agreement of TB-mBJ calculations with reported scales and obtained fine accuracy levels is reason for detailed illustration across high symmetry directions. It may also be noticed that the energy band gap obtained from TB-mBJ computations are adjacent to ideal defined value (≈1.5 eV) for solar photovoltaic application and further provides the optimum results when compared with earlier reported data (Table 2). It may also be noted that best to our knowledge there is no reported data on the electronic properties of $KSnBr_3$. Further, for the studied perovskite compounds, direct band gap nature is depicted from Fig. 3(a–d). For all the compounds, valence band maximum (VBM) and conduction band minimum (CBM) lies at R (0.5, 0.5, 0.5) point of the first BZ. From Fig. 3(a–d), it is also observed that overall shape of energy bands for Br based perovskite compounds are similar to that of Cl based compounds. Further, it is also observed that the band gap of material reduces when Cl is replaced with Br. This is in accordance with the earlier reported data (Table 2). This reduction in band gap of the material improves optical performance for photo-voltaic applications which is explained in terms of absorption spectra of these compounds in next section. Except some fine structure and energy values, band structure for $RbSnCl(Br)_3$ obtained in present computations are similar to the earlier reported calculations [26,29]. The results obtained for the energy band structure depicts almost same energy gap for Rb and K based tin halide perovskites, which is in accordance with the earlier reported data [24]. It may be noted that there is no available data on the energy gap or electronic properties of $KSnBr_3$. Further, for clarity we have plotted energy band structures in colored mode to specifically

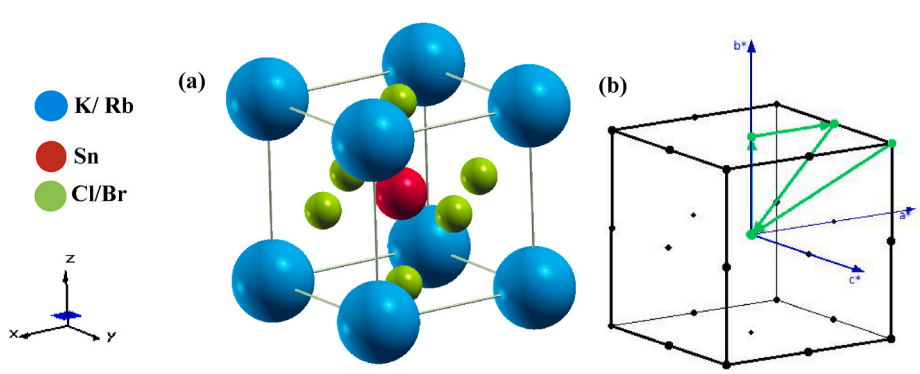

Fig. 2. (a) Crystal Structure and (b) Brillion zones along with high symmetry directions for $ASnX_3$ (A = Rb/K); (X = Cl/Br).

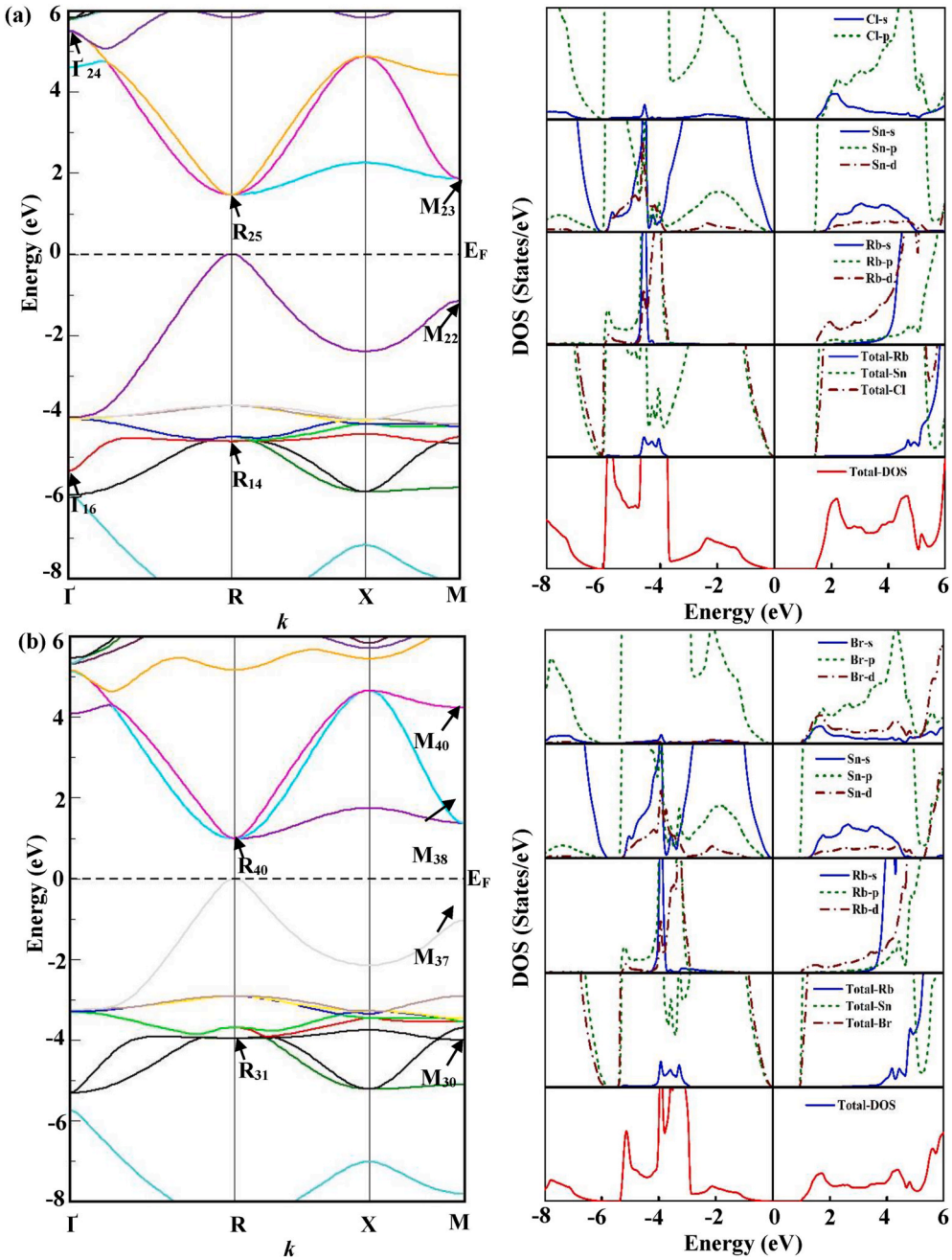

Fig. 3. (Color online) Energy bands, total and partial density of states plotted using TB-mBJ scheme for (a) $RbSnCl_3$ (b) $RbSnBr_3$ (c) $KSnCl_3$ and (d) $KSnBr_3$. All computations are performed along high symmetry directions of the first Brillouin Zone. Featured k points selected along high symmetry directions are Γ (0,0,0); R (0.5, 0.5, 0.5); X (0,0.5,0) and M (0.5,0.5, 0).

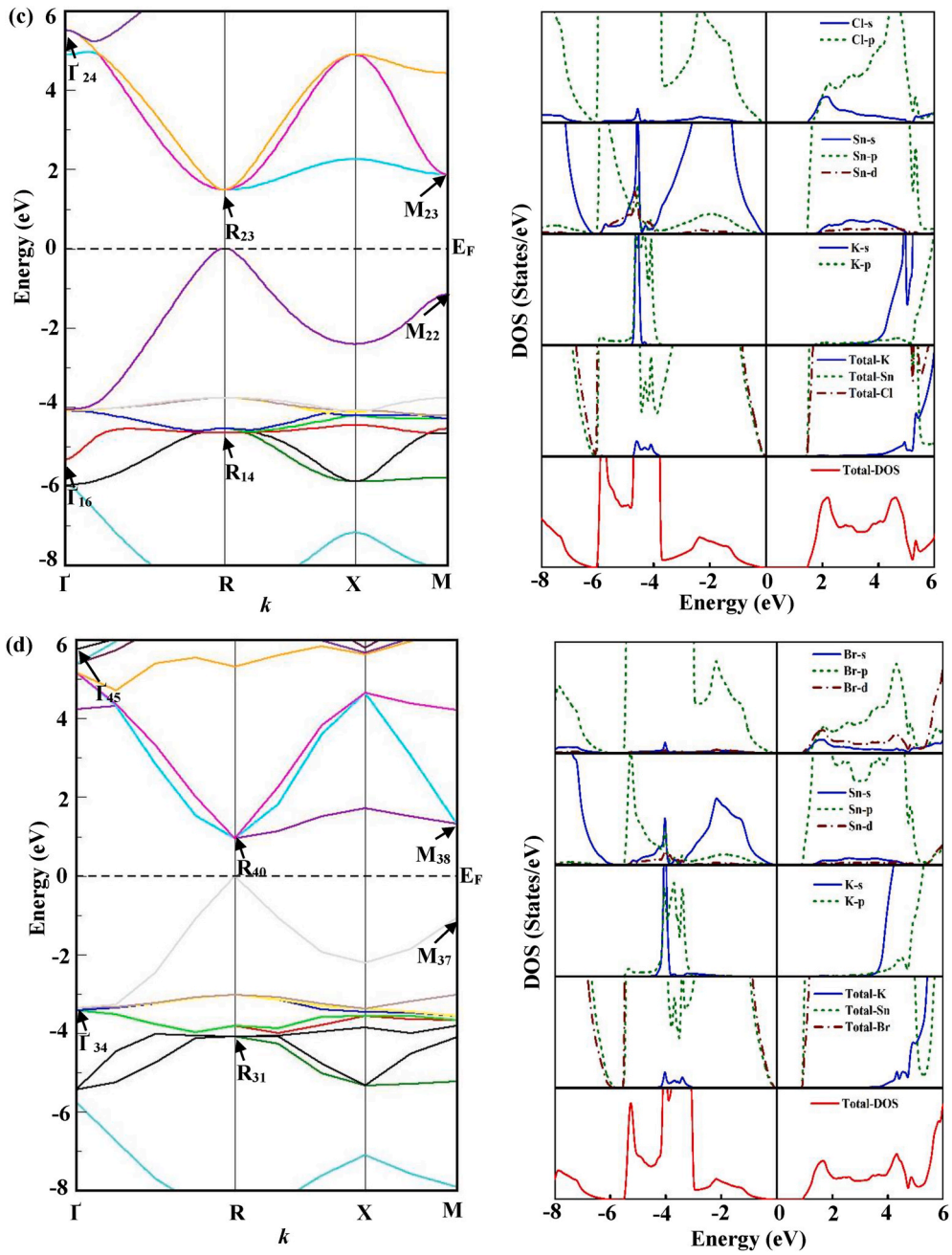

Fig. 3. (*continued*).

indicate discrete energy states occupied by the available electrons. It is worth mentioning that, for the detailed investigations of the formation of energy bands, one need to compute the total and partial density of states (DOS). Therefore, we have also presented the DOS for $ASnX_3$ (A = Rb, K; X = Cl, Br) compounds in Fig. 3(a–d) which are in well reconciliation with available results [26,29]. It is observed that, when Cl is replaced with Br, DOS spectra shifts towards lower energy side in conduction region which results in the reduction of energy gap of material. Energy bands obtained for (Rb, K)$SnCl_3$ perovskite observed in valence band just below the Fermi level (E_F) and bands in the conduction band (CB) are majorly resulted due to hybridization of Sn (5sp) and Cl (3sp) states along with the small traces of Rb (4sp and 3d) and K (3sp). Similarly, bands observed for (Rb,K)$SnBr_3$ are influenced with major contribution of Sn (5sp & 4d) and Br (4sp) along with minor insertions of Rb (4sp & 3d) and K (3sp) states. Since, the bands in deep core region, do not contribute in any of electronic and optical properties of materials, hence we are skipping their discussion. But in the same manner, concentration of different band structure regions can be elaborated, and reasonable measures may be adopted for necessary improvements.

3.2. Optical properties

Investigations of optical properties of $ASnX_3$ (A = Rb, K; X = Cl, Br) perovskite compounds, enable us to precisely illustrate their probable utilization in various opto-electronic applications. As mentioned above, the energy gap computed using TB-mBJ for all the studied compounds

Table 2
Energy band gap (Eg) eV of $ASnX_3$ (A = Rb, K); (X = Cl, Br) using PBE-GGA and TB-mBJ along with available theoretical data.

Perovskite Compounds	Technique	Present Work	Available Data
$RbSnCl_3$	TB-mBJ	1.46	[a]1.61,[b]0.94,[c]1.43,[e]1.44
	PBE-GGA	0.88	
$RbSnBr_3$	TB-mBJ	0.98	[a]1.10,[b]0.59,[d]0.57
	PBE-GGA	0.61	
$KSnCl_3$	TB-mBJ	1.48	[c]1.37,[e]1.24
	PBE-GGA	0.89	
$KSnBr_3$	TB-mBJ	0.93	
	PBE-GGA	0.57	

[a] Körbel et al. (2016).
[b] Jain et al.(2019).
[c] Mao et al. (2018).
[d] Benyahia et al.(2019).
[e] Yi et al.(2019).

are in better reconciliation with earlier reported theoretical data, computations for comprehensive optical properties such as, real and imaginary dielectric tensor components, absorption coefficient, reflectivity and refractivity spectra are performed using the TB-mBJ method only.

Most relevant frequency dependent complex dielectric function '$\varepsilon(\omega)$' is studied to explore the optical impedance of medium during the electromagnetic interaction. The complex dielectric function is represented as:

$$\varepsilon_{\alpha\beta}(\omega) = \varepsilon_1(\omega) + i\,\varepsilon_2(\omega), \tag{4}$$

here, '$\varepsilon_1(\omega)$' and '$\varepsilon_2(\omega)$' stands for the real and imaginary components of dielectric tensor, respectively. It is worth mentioning that real and imaginary components of '$\varepsilon(\omega)$' indicates the amount of energy stored in any medium and the energy loss during absorption of sunlight, respectively. Mathematically, real and imaginary dielectric tensor components are represented as:

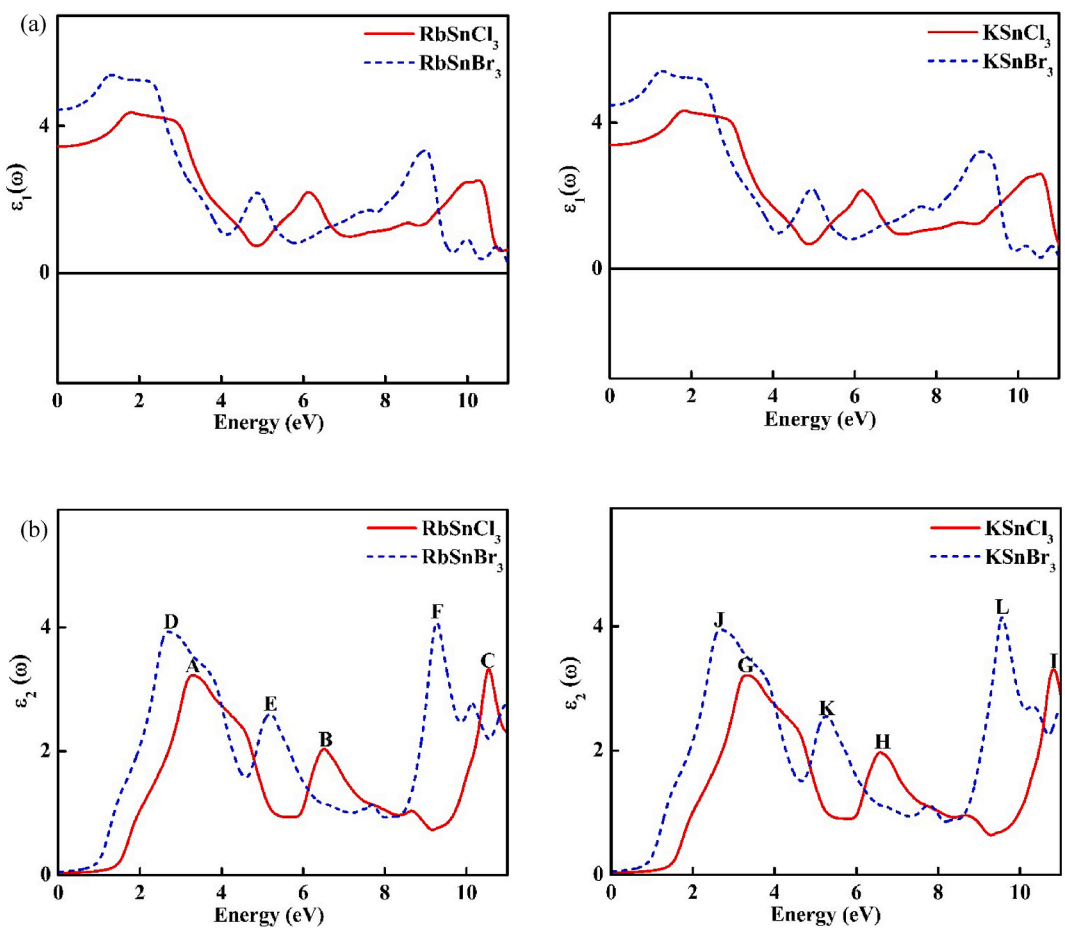

Fig. 4. (Color online) Frequency dependent (a) real $\varepsilon_1(\omega)$and (b) imaginary$\varepsilon_2(\omega)$dielectric tensor components drawn for $(Rb,K)Sn(Cl,Br)_3$ obtained from TB-mBJ approximation.

Table 3
Peak positions in $\varepsilon_2(\omega)$spectra, together with possible dominant transition in energy bands.

Perovskite Samples	Peaks	Peak Position (eV)	Dominant Transitions	Perovskite Samples	Peaks	Peak Position (eV)	Dominant Transitions
$RbSnCl_3$	A	3.2	$M_{22} \rightarrow M_{23}$	$KSnCl_3$	G	3.3	$M_{23} \rightarrow M_{22}$
	B	6.5	$R_{14} \rightarrow R_{25}$		H	6.5	$R_{14} \rightarrow R_{23}$
	C	10.5	$\Gamma'_{16} \rightarrow \Gamma'_{24}$		I	10.8	$\Gamma'_{16} \rightarrow \Gamma'_{24}$
$RbSnBr_3$	D	2.5	$M_{37} \rightarrow M_{38}$	$KSnBr_3$	J	2.5	$M_{37} \rightarrow M_{38}$
	E	5.2	$R_{31} \rightarrow R_{40}$		K	5.2	$R_{31} \rightarrow R_{40}$
	F	9.2	$M_{29} \rightarrow M_{40}$		L	9.5	$\Gamma'_{34} \rightarrow \Gamma'_{45}$

Table 4
Calculated optical constants: Dielectric constant $\varepsilon_1(0)$, refractive index $\eta(0)$and reflectivity $R(0)$ for ASnX3 (A = Rb, K) and (X = Cl, Br) perovskite compounds.

Perovskite Samples	$\varepsilon_1(0)$	$\eta(0)$	R (0)
$RbSnCl_3$	3.44	1.85	0.089
$RbSnBr_3$	4.44	2.11	0.127
$KSnCl_3$	3.39	1.84	0.087
$KSnBr_3$	4.48	2.12	0.128

$$\varepsilon_1(\omega) = \mathrm{Re}\,[\varepsilon_{\alpha\beta}(\omega)] = \delta_{\alpha\beta} + \frac{2}{\pi} P \int_0^\infty \frac{\omega' \,\mathrm{Im}\,[\varepsilon_{\alpha\beta}(\omega')]}{\omega'^2 - \omega^2} d\omega' , \tag{5}$$

$$\varepsilon_2(\omega) = \mathrm{Im}\,[\varepsilon_{\alpha\beta}(\omega)] = \frac{4\pi e^2}{m^2\omega^2} \sum_{v,c} \int_{BZ} dk \langle c_k\,|p^\alpha|\,v_k\rangle\,\langle v_k\,|p^\beta|\,c_k\rangle|\delta\,(\varepsilon_{ck} - \varepsilon_{ck} - \omega), \tag{6}$$

here, 'k' represents the wave vector, whereas 'c_k' and 'v_k' represents the crystal wave functions for conduction band and valence band respectively. The computed $\varepsilon_1(\omega)$ and$\varepsilon_2(\omega)$ spectra for perovskites (Rb, K)Sn (Cl, Br)$_3$ compounds are presented in Fig. 4 (a, b). Further, it is worthwhile to mention that the various peaks appearing in imaginary dielectric tensor are the result of electronic transitions and can be explained through inter-band transitions occurred between valence and conduction bands. Peak positions along with possible dominant transitions for all the studied perovskite compounds, are collated in Table 3. Optical peaks for perovskite materials (Rb, K)$SnBr_3$ are appearing at different energy value. Dominant transitions corresponding to each peak can be explained in coordination with respective energy band structures (Fig. 3). For example, peak at 2.5 eV energy, leveled as D, J (Fig. 4b), are possibly occurred due to electron transition between Sn (5s) and Br (4p) states and are indicated as $M_{37} \rightarrow M_{38}$ transitions in Fig. 3 (b, d). Similarly, peaks E, K appearing at 5.2 eV (Fig. 4b) may be due to transition from $R_{31} \rightarrow R_{40}$ which corresponds to electronic transition between Sn (5s) and Br (3d) states. Further, peaks resulted at 9.2 eV and 9.5 eV energy, leveled as F, L in Fig. 4b, are elucidated when transition takes place amongst Rb (5s) → Sn (5p) ($M_{29} \rightarrow M_{40}$) and K (3p) → Br (3d) states ($\Gamma'_{34} \rightarrow \Gamma'_{45}$) respectively. In the similar manner, remaining peaks can also be explained by comparing imaginary tensor (Fig. 4b) and corresponding band structures (Fig. 3a and c). In real part of dielectric tensor, static constant at 0 eV energy is the most important parameter which depends upon the energy gap of material and has inverse relation with the energy gap of the material. The values obtained for $\varepsilon_1(0)$, are presented in Table 4 for all the studied perovskite compounds. This may be noted that values resulted for $\varepsilon_1(0)$ are higher for (Rb, K)$SnBr_3$ in comparison to (Rb, K)$SnCl_3$ compounds which is also in agreement with Penn model [39].

The knowledge of dielectric function is sufficient to understand the other important optical parameters such as, absorption coefficient $\alpha(\omega)$, refractive index $\eta(\omega)$ and reflectivity spectra $R(\omega)$. All these parameters can be explained in terms of $\varepsilon_1(\omega)$ and $\varepsilon_2(\omega)$. Mathematically,

$$\alpha(\omega) = \left[\frac{2\omega\, k(\omega)}{c}\right] \tag{7}$$

where, $k(\omega)$ is the extinction coefficient which is represented as:

$$k(\omega) = \sqrt{\frac{\varepsilon_1^2(\omega) + \varepsilon_2^2(\omega) - \varepsilon_1(\omega)}{2}} \tag{8}$$

$$\eta(\omega) = \frac{1}{\sqrt{2}} \sqrt{\{\varepsilon_1(\omega)^2 + \varepsilon_2(\omega)^2\}^{1/2} + \varepsilon_1(\omega)}, \tag{9}$$

$$R(\omega) = \frac{[n(\omega) - 1]^2 + k(\omega)^2}{[n(\omega) + 1]^2 + k(\omega)^2}, \tag{10}$$

Absorption spectra computed for (Rb, K)Sn Cl, Br)$_3$ are presented in Fig. 5 (a, b), which indicates sufficient absorption in visible energy range (0–5 eV) and affirms the potential utilization of studied compounds in photo-voltaic applications. Further, $MAPbI_3$ (MA = CH_3NH_3) hybrid perovskite compound is the well known potential compound for the photovoltaic applications, we have compared the absorption spectra of $MAPbI_3$ with the studied (Rb/K)Sn(Cl,Br)$_3$ compounds (Fig. 5). Optical performance for specific material is accomplished through evaluation of integrated absorption coefficient (IAC) and obtained results collated here in Table 5 along with the IAC for available data [8,9] of $MAPbI_3$. Calculated IAC values, revealed higher absorption potential for (Rb,K) $SnBr_3$ perovskites when compared with Cl based materials and hence proposed to have good optical combability. Optical response of any material can also be explained in terms of frequency dependent reflectivity [$R(\omega)$] and refractivity [$\eta(\omega)$] spectra which are presented in Fig. 6

Table 5
Integrated absorption coefficient (IAC) for $ASnX_3$ (A = Rb, K); (X = Cl, Br) and $MAPbI_3$ (MA = CH_3NH_3) in 0–5 eV energy range.

Samples	IAC (x10^4 eV/cm)	Samples	IAC (x10^4 eV/cm)
$RbSnCl_3$	80.060	$KSnCl_3$	80.262
$RbSnBr_3$	90.186	$KSnBr_3$	90.269
[a]$MAPbI_3$ [8]	26.23	[a]$MAPbI_3$ [9]	118.36

[a] Available data [8,9].

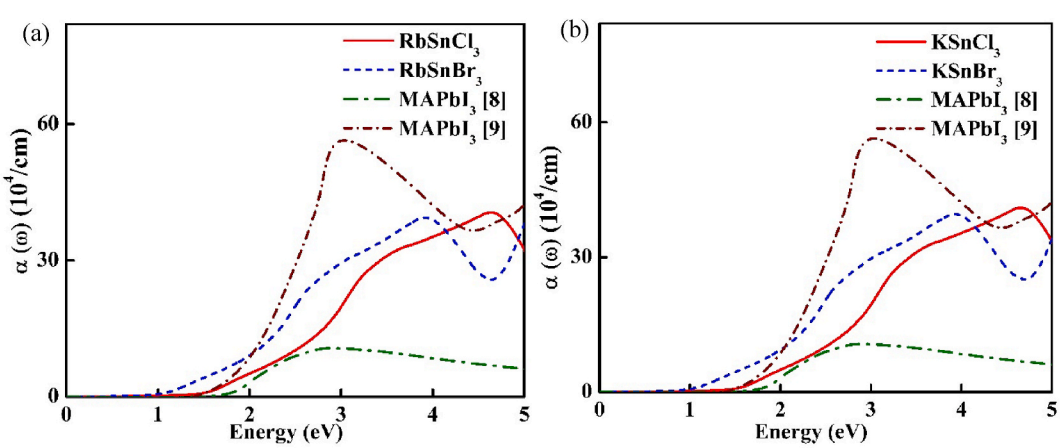

Fig. 5. (Color online) Absorption spectra $\alpha(\omega)$for (a) RbSn(Cl,Br)$_3$ and (b) KSn(Cl,Br)$_3$ from TB-mBJ approximation alongwith the for $CH_3NH_3PbI_3$ taken from earlier reported data (Ref. 8, 9).

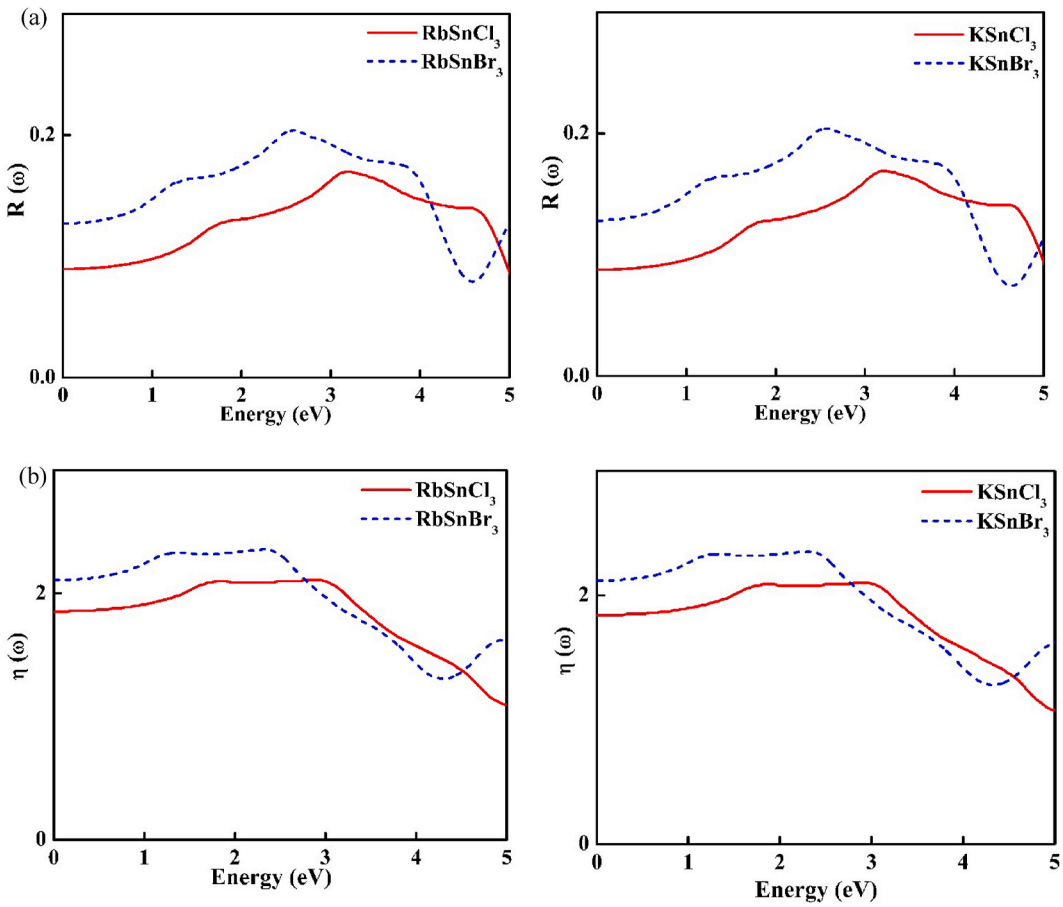

Fig. 6. (Color online) Energy dependent (a) Reflectivity$R(\omega)$and (b) Refractivity $\eta(\omega)$ spectra calculations for (Rb,K)Sn(Cl,Br)$_3$ obtained from TB-mBJ approximation.

(a,b) for all the studied compounds. The possible candidature of any compound as perfect absorber completely depends upon their reflectance and reflectivity spectra. Further, for better optical response summation of absorption (A), refraction (T) and reflectance (R) should be equal to 1. Optical responses obtained at zero frequency for reflectivity $[R(0)]$ and refractivity $[\eta(0)]$ spectra are collated in Table 4. Precision investigations indicates 25% better optical performance for (Rb,K)SnBr$_3$ perovskites and hence suggest these more suitable for future opto-electronic and photo-voltaic applications.

4. Conclusions

In this work, density functional investigations for lead-free metal tin halide perovskite ASnX$_3$ (A = Rb, K; X = Cl, Br) compounds are performed by using the utmost precise full potential linearized augmented plane wave (FP-LAPW) method as embodied in Wien2k code. Detailed behavior analysis performed includes structural optimization, band structure, density of states, real & imaginary dielectric tensor, optical absorption, reflectivity and refractivity spectra for studied compounds using the Tran-Blaha modified Becke-Johnson (TB-mBJ) exchange and correlation potential. Direct band gap magnitudes observed for chosen perovskite materials KSnCl$_3$ (KSnBr$_3$) and RbSnCl$_3$ (RbSnBr$_3$) are 1.48 (0.93) and 1.46 (0.98) eV, respectively. Decent agreement of TB-mBJ computations with previously available results confirms accuracy of present computations. Reduced band gap, improved absorption spectra (0–5 eV) and enhanced integrated absorption coefficient (IAC) recorded while switching from X = Cl to Br revealed promising nature of (Rb,K) SnBr$_3$ perovskite materials for effective utilization in future photovoltaic applications.

CRediT authorship contribution statement

Karina Khan: Investigation, Methodology, calculation. **Jagrati Sahariya:** Conceptualization, Writing - review & editing, Supervision. **Amit Soni:** Writing - review & editing, Funding acquisition, from SERB.

Declaration of competing interest

The authors declare that they have no known competing financial interests or personal relationships that could have appeared to influence the work reported in this paper.

Acknowledgement

Researchers involved are immensely grateful to Prof. P. Blaha of the Vienna University group for providing Wien2k code and Manipal University Jaipur for providing all necessary arrangements. This work is financially supported by DST-SERB, New Delhi (India), vide grant number EMR/2017/005534.

References

[1] N. Kannan, D. Vakeesan, Renew. Sustain. Energy Rev. 62 (2016) 1092–1105.
[2] T.D. Lee, A.U. Ebong, Renew. Sustain. Energy Rev. 70 (2017) 1286–1297.
[3] H. Zhang, Y. Lu, W. Han, J. Zhu, Y. Zhang, W. Huang, Chem. Eng. J. 393 (2020) 124766.
[4] C. Gai, J. Wang, Y. Wang, J. Li, Energies 13 (2020) 2–26.
[5] N.K. Noel, S.D. Stranks, A. Abate, C. Wehrenfennig, S. Guarnera, A.A. Haghighirad, A. Sadhanala, G.E. Eperon, S.K. Pathak, M.B. Johnston, A. Petrozza, L.M. Herza, H. J. Snaith, Energy Environ. Sci. 7 (2014) 3061–3068.
[6] Y. Ye, X. Run, X.H. Tao, H. Feng, X. Fei, W.L. Jun, Chin. Phys. B 24 (2015) 116302.

[7] Y.Q. Zhao, Q.R. Ma, B. Liu, Z.L. Yu, J. Yang, M.Q. Cai, Nanoscale 10 (2018) 8677–8688.
[8] M. Roknuzzaman, K. Ostrikov, K.C. Wasalathilake, C. Yan, H. Wang, T. Tesfamichael, Org. Electron. 59 (2018) 99–106.
[9] A. Shukla, V.K. Sharma, S.K. Gupta, A.S. Verma, Mater. Res. Express 6 (2019) 126323.
[10] Y.Q. Zhao, Y. Xu, D. F Zou, J.N. Wang, G.F. Xie, B. Liu, M.Q. Cai, S.L. Jiang, J. Phys. Condens. Matter 32 (2020) 195501.
[11] D.N. Yan, C.S. Liao, Y.Q. Zhao, B. Liu, J.L. Yang, M.Q. Cai, J. Phys. D Appl. Phys. 53 (2020) 1–38.
[12] A. Soni, K.C. Bhamu, J. Sahariya, J. Alloys Compd. 817 (2020) 152758.
[13] Z.L. Yu, Q.R. Ma, B. Liu, Y.Q. Zhao, L.Z. Wang, H. Zhou, M.Q. Cai, J. Phys. Appl. Phys. 50 (1 – 27) (2017) 405101.
[14] J. Zhang, J. Su, Z. Lin, M. Liu, J. Chang, Y. Hao, Appl. Phys. Lett. 114 (1 – 5) (2019) 181902.
[15] M. Konstantakou, T. Stergiopoulos, J. Mater. Chem. 5 (2017) 11518–11549.
[16] K.A. Parrey, T. Farooq, S.A. Khan, U. Farooq, A. Gupta, Computational Condensed Matter 16 (1 – 8) (2019), e00381.
[17] Y. Li, X. Gong, P. Zhang, X. Shao, Chem. Phys. Lett. 716 (2019) 76–82.
[18] T. Krishnamoorthy, H. Ding, C. Yan, W.L. Leong, T. Baikie, Z. Zhang, M. Sherburne, S. Li, M. Asta, N. Mathews, S.G. Mhaisalkar, J. Mater. Chem. 3 (2015) 23829–23832.
[19] S. Körbel, M.A.L. Marques, S. Botti, J. Mater. Chem. C 4 (2016) 3157–3167.
[20] J. Young, J.M. Rondinelli, J. Phys. Chem. Lett. 5 (2016) 918–922.
[21] W. Travis, E.N.K. Glover, H. Bronstein, D.O. Scanlon, R.G. Palgrave, Chem. Sci. 7 (2016) 4548–4556.
[22] G. Gou, J. Young, X. Liu, J.M. Rondinelli, Inorg. Chem. 56 (2017) 26–32.
[23] Y. Jung, J. Lee, A. Walsh, A. Soon, Chem. Mater. 7 (2017) 3181–3188.
[24] X. Mao, L. Sun, T. Wu, T. Chu, W.Q. Deng, K. Han, J. Phys. Chem. C 14 (2018) 7670–7675.
[25] J. Jiang, C.K. Onwudinanti, R.A. Hatton, P.A. Bobbert, S. Tao, J. Phys. Chem. C 122 (2018) 17660–17667.
[26] D. Jain, S. Chaube, P. Khullar, S.G. Srinivasan, B. Rai, Phys. Chem. Chem. Phys. 21 (2019) 19423–19436.
[27] L. Yunsheng, G. Xu, Z. Peihuan, S. Xiaohong, Chem. Phys. Lett. 716 (2019) 76–82.
[28] Q. Mahmood, M. Yaseen, M. Hassan, M.S. Rashid, I. Tlili, A. Lareff, Mater. Res. Express 6 (2019) 1–25.
[29] K. Benyahia, S. Bouchikhi, S. Bekhechi, Phys. Sci. Biophys. Journal 3 (2019) 1–6.
[30] Z. Yi, N.H. Ladi, X. Shai, H. Li, Y. Shen, M. Wang, Nanoscale Advances 1 (2019) 1276–1289.
[31] R. Yang, J.M. Skelton, E. Silva, J.M. Frost, A. Walsh, J. Chem. Phys. 152 (2020) 1–10, 024703.
[32] M. Kar, T. Körzdörfer, Mater. Res. Express 7 (2020) 1–10, 055502.
[33] P. Blaha, K. Schwarz, G.K.H. Madsen, D. Kvasnicka, J. Luitz, Wien2k-An Augmented Plane Wave Plus Local Orbitals Program for Calculating Crystal Properties, Vienna University of Technology, Vienna, Austria, 2016.
[34] W. Kohn, L.J. Sham, Phys. Rev. 140 (1965) 1133–1138.
[35] J.P. Perdew, K. Burke, M. Ernzerhof, Phys. Rev. Lett. 77 (1996) 3865–3868.
[36] F. Tran, P. Blaha, Phys. Rev. Lett. 102 (1 – 4) (2009) 226401.
[37] D. Koller, F. Tran, P. Blaha, Phys. Rev. B 83 (1 – 10) (2011) 195134.
[38] L. Mehdaouia, R. Miloua, M. Khadraoui, M.O. Bensaid, D. Abdelkader, F. Chiker, A. Bouzidi, Phys. B Condens. Matter 564 (2019) 114–124.
[39] D.R. Penn, Phys. Rev. 128 (1962) 2093–2097.